九州大学大学院総合理工学報告
第32巻 第4号 1-8頁 平成23年2月

Engineering Sciences Reports, Kyushu University
Vol. 32, No. 4, pp. 1-8, FEB, 2011

A scale-model experiment of surface temperature characteristics using an infrared radiation camera

Joao Tales Oliveira*1,†, Aya Hagishima*2, Jun Tanimoto*3

†E-mail of corresponding author: *es308021@s.kyushu-u.ac.jp*

(Received January 31, 2011)

An outdoor measurement was performed during fine weather with a scale-model array of cubical obstacles (size 100mm, 25% packing density, lattice-type square layout) that represent an idealized urban tissue. Surface temperature was recorded with high-frequency (10Hz) infrared camera, along with wind speed and solar radiation. Complementarily, air temperature was also measured at three heights in the near-wall region of a block surface using fine-wire thermocouples. Results showed the similarity of distribution between surface temperature and scalar transfer coefficient. We also found that 10s averaging period may be appropriate for the analysis of surface temperature fluctuation affected by turbulent airflow. In the near-wall region under particularly calm wind condition, air temperature fluctuation caused by a hot plume arising from the warmed surface was observed. The method presented in this study seems to be a promising tool to analyze surface temperature characteristics of scale-models in urban climate studies.

Key words : *infrared thermography, field measurement, urban-like block array*

1. Introduction

Micro-climate in urban areas is a very complex phenomenon with direct implications in people's daily life, comfort, and health. This complexity is derived from myriad interactions of physical processes. Various types of field measurement in urban areas allow for many contributions .[1] Its merit lies in acquiring data under real atmospheric conditions – solar radiation, precipitation, atmospheric stability, large scale turbulence – which in turn give realistic features from the viewpoints of boundary layer aerodynamics. However, field measurements posit many difficulties: they are usually costly, require careful logistics, and can be hindered by traffic or other factors inherent to public spaces. For these reasons, some researchers opt to use small-scaled physical models as an alternative (Kanda, 2006) [2] . Some of these studies are conducted in wind tunnels, others are conducted outdoors.

Wind tunnel experiments have been conducted to mainly grasp turbulent structures within and above urban canopy layer under neutral conditions, whereas outdoor scale model experiments have contributed to investigate more various aspects of urban climate in a real setting. Aida[3] examined the effect of urban surface irregularity on albedo. Oke[4] investigated nocturnal cooling rates for rural and urban environments under calm and cloudless conditions. In addition, experiments have been conducted mainly driven by the need to understand energy balance of urban areas [5] ,[6] air flow within street canyon, and scalar dispersion [7] [8] . Still, the effect of flow on spatial distribution of urban surface is not well investigated.

Scale-models cannot provide the data under a real urban setting with complex geometry and mixture of various materials like field measurements in urban areas. However they have the advantage of allowing systematic investigation of factorial effects, such as urban geometry, material of urban surfaces, and size, on urban thermal balance, resulting in important insights about the mechanism of urban climate.In addition, scale model experiments generally facilitate to perform multi-point extensive measurement of various physical variables, such as temperature of air and urban surfaces, radiation flux, sensible heat flux, and turbulent statistics. It is effective to examine highly heterogeneous urban streets.

Meanwhile, understanding of momentum and

*1 Department of Energy and Environmental Engineering
*2 Department of Energy and Environmental Engineering
*3 Department of Energy and Environmental Engineering

scalar transfer process on a rough wall are important issues to not only urban climatology but also various engineering fields and fluid dynamics. For example, Cheng and Castro[9] performed comprehensive measurements of profiles of mean wind and turbulent statistics over block arrays in a wind tunnel. Kovar-Panskus[10] measured airflow within a two-dimensional street canyon to investigate the influence of solar-induced wall heating on the airflow pattern.

In the light of these facts, the aim of this study is to challenge to observe temperature distribution and its fluctuation on a cubical array using infrared thermography. It allows the analysis of surface temperature without disturbing the flow. Although it is already used in flow visualization [11] , these studies are conducted mainly indoors, without taking into account the effect of solar radiation. Complementarily, air temperature in near-wall regions of a block surface was measured by fast-response thermocouples to grasp the characteristics of the thermal boundary layer developed over urban roughness.

2. Experiment setup

2.1 Scale-model details

The experiment was done in an open space inside Chikushi Campus of Kyushu University. It is located in the city of Kasuga, Japan, latitude 33.52°north and longitude 130.48°East. The site was an unobstructed area between two buildings and unshaded during measurement period. Figure 1 shows a sketch of the experiment setup, and fig. 2 shows the measurement site.

81 cubical obstacles with a size of 100 mm (hereafter, H) were arranged in lattice-type square layout with 25% packing density on a board with 100mm thickness. Both the obstacles and the board are made of polyurethane foam , commonly used as insulation in building envelopes. Twenty five obstacles at the center of the array were covered with 0.3mm aluminum sheet, coated with matte black paint. The surface area of the board under these 25 obstacles was also covered with the same material (gray area shown in fig. 1), thus creating an homogenous 3-dimensional array. The remaining obstacles were left uncovered. The choice of material (thin aluminum sheet + polyurethane) and color (matte black) allows high surface emissivity (we assumed $\epsilon = 1$, and adjusted the camera accordingly), low heat capacity, and a quick temperature response.

2.2 Measurement and instrumentation

Surface temperature distribution of the array was measured with a frequency of 10Hz using a portable infrared camera (Nippon Avionics TVS-200). The camera has a temperature resolution of 0.08℃, and accuracy of ±2℃. It enables to output the data into images with 320 x 240 pixels that can be processed through computation. To protect from direct sunlight, a cardboard box covered with high-reflective tape was placed over it during all experiments. During measurements, the camera was placed facing the board at a height of approximately one meter.

Simultaneously, air temperature was acquired using fine-wire thermocouples (⌀=0.0127mm) placed at different heights – 1mm, 5mm, 10mm – in order to investigate the thermal profile above a roof of a block. Three-dimensional airflow was measured using two ultrasonic anemometers placed at 2H (anemometer A – Kaijo WA(T)395) and 10H (anemometer B – Young 81000), respectively. Solar radiation was measured with a pyranometer (EKO MS-602) placed in a clear area near the site. The measurement frequency of the anemometers and the pyranometer was synchronized with that of the camera.

2.3 Measurement period

The experiment was conducted on several days, under different weather conditions according to table 1. The last experiment (2010/01/10), which has no missing data from the thermocouples, was selected for the following analysis. There were two experiments in that day, hereafter called as exp01 and exp02.

Table 1 Measurement period. $\bar{I_{sr}}$: mean solar radiation $[W/m^2]$; $\bar{u}$: mean wind speed $[m/s]$; α: solar angle at the time [degree].

Date	Start	End	$\bar{I_{sr}}$	$\bar{u}$	α	Label
9/16	12:00	12:30	629	0.81	59.03	–
	13:41	14:11	551	0.95	50.32	–
	15:16	15:46	177	1.00	34.71	–
9/17	12:00	12:30	820	0.53	58.66	–
	13:37	14:07	721	0.90	49.95	–
	15:14	15:44	526	0.85	34.39	–
9/18	12:00	12:30	823	0.60	58.28	–
	13:42	14:17	704	0.55	49.59	–
	15:32	16:07	336	0.83	30.20	–
10/1	10:46	11:25	764	0.51	50.02	exp01
	12:47	13:26	737	0.54	50.52	exp02

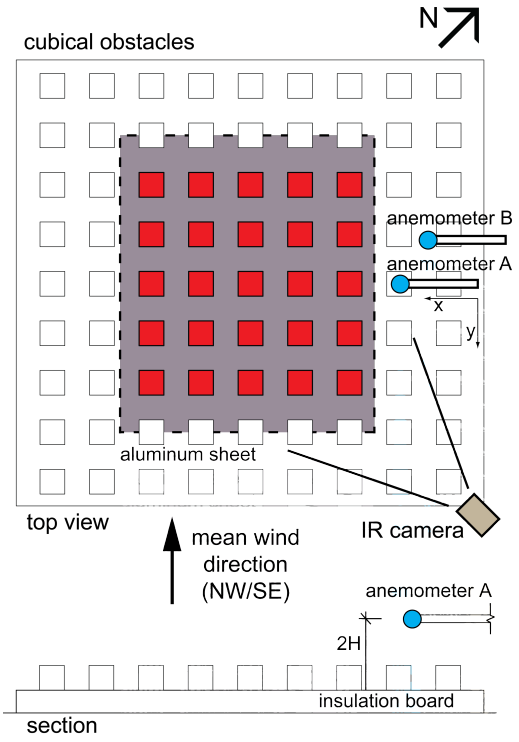

Fig. 1 Experiment setup. Red squares represents covered obstacles; Gray area represents aluminum sheet laid on the insulation board. The blue dot represents the probe's position.

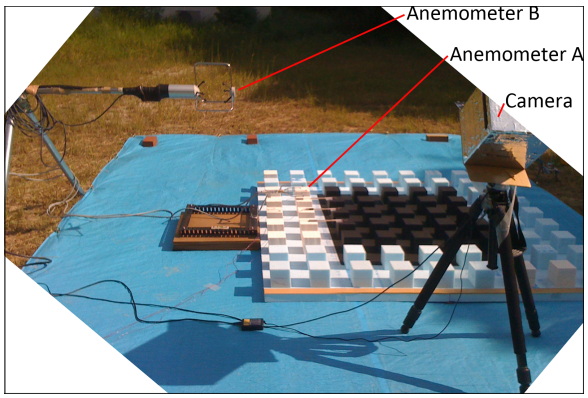

Fig. 2 Experiment site of this study.

3. Results and discussion

3.1 Climate conditions

Background climate conditions from anemometer A are shown in figs. 3 and 4. It was a clear day with little variation of global solar radiation except for a brief interval of cloud cover by the end of exp02 (fig. 4, at 13:21). In general, wind speed was relatively calm, the mean value for the two experiments were 0.5 m/s.

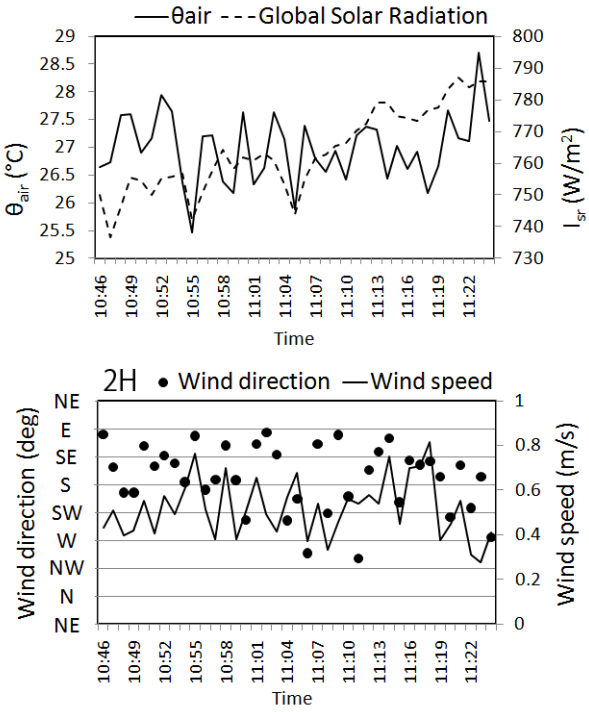

Fig. 3 Weather conditions for exp01 (10:47 to 11:25 – 38 min). Values averaged for a period of one minute.

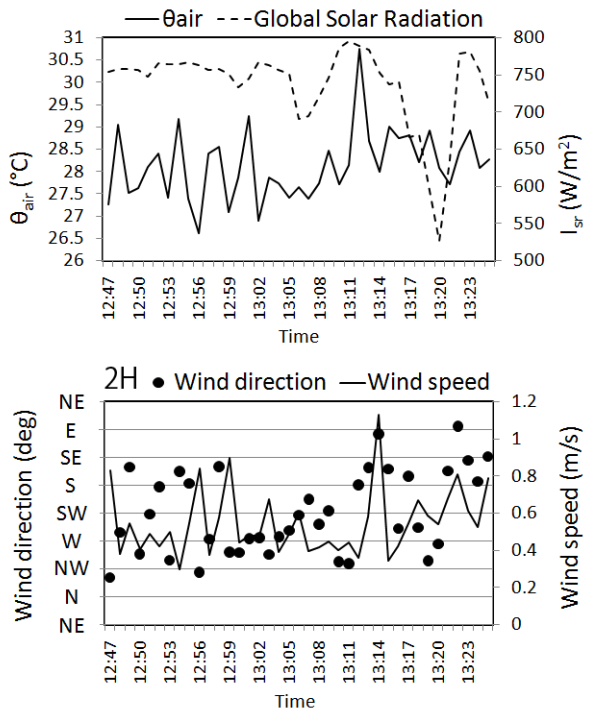

Fig. 4 Weather conditions for exp02 (12:47 to 13:26 – 39 min). Values averaged for a period of one minute.

3.2 Mean surface temperature

Figures 5 and 6 show the thermal images from the IR camera for exp01 and exp02, respectively. We adopt surfaces with different orientations for analysis: roof and street (horizontal), wall A (exposed to incident solar radiation) and wall B (shaded surface).

As can be inferred from table 1, in spite of the almost same conditions of solar radiation and air temperature, there are differences in mean surface temperature distribution, which could be caused by the change in solar position with time.

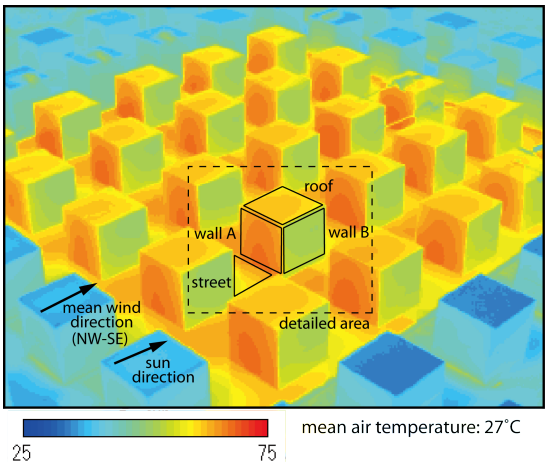

Fig. 5 Distribution of mean surface temperature of the array for the entire period of exp01. The areas named roof, wall A, wall B, and street are delimited by black polygons.

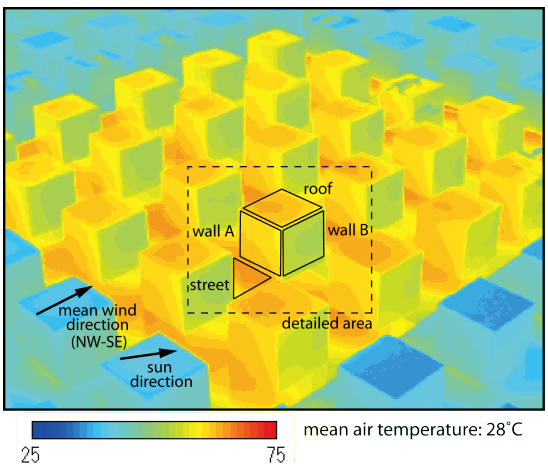

Fig. 6 Distribution of mean surface temperature of the array for the entire period of exp02. The areas named roof, wall A, wall B, and street are delimited by black polygons.

Figures 7 and 8 show for one minute the spatial-temporal average of surface temperature of each surface against solar radiation and wind speed, respectively, for the entire period of exp01 and exp02. There is no clear correlation between solar radiation and surface temperature because of stable solar radiation during all measurement period except for several minutes. Thus, the effect of solar radiation on surface temperature for each surface is probably negligible.

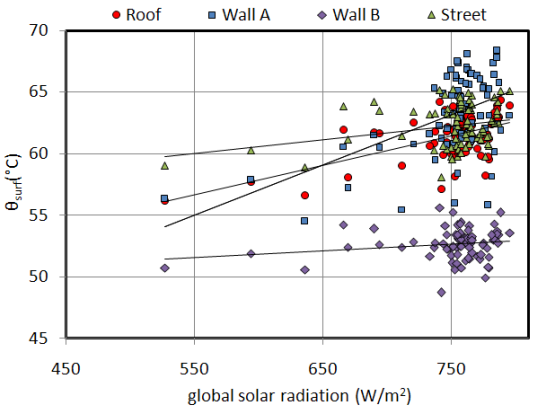

Fig. 7 Spatial-temporal average of surface temperature for roof, wall A, wall B and street, vs solar radiation. Averaged one minute values for the entire period of exp01 and exp02.

In contrast, the negative correlation between surface temperature and wind speed is evident. The slopes of roof, wall A, and wall B are not much different, whereas the slope of street is the smallest. Because the street is at the bottom of the cavity, and it is less subject to the flow above the canopy.

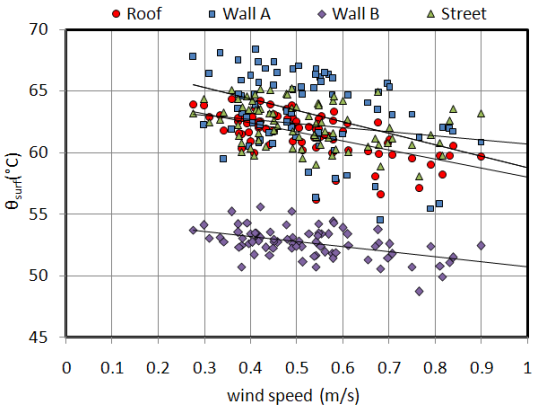

Fig. 8 Spatial-temporal average of surface temperature for roof, wall A, wall B and street, vs wind speed. Averaged one minute values for the entire period of exp01 and exp02.

To narrow the period for analysis, we picked up

one particular minute according to the following criteria: *mostly* mild wind conditions (between 0.3 and 0.6 m/s), stable global solar radiation (standard deviation of less than 3 W/m^2), and relatively stable wind direction perpendicular to the street (NW-SE, see fig. 1). The one-minute period at 13:04 was chosen for its range of wind conditions (mostly mild – 0.4 m/s – but with relatively high – 1.2 m/s – and low peaks – 0.2 m/s), which might be suitable for investigation of surface temperature reaction to fluctuation of airflow in a brief interval of time. The subsequent sections will show results based on this period.

3.3 Surface temperature characteristics

Figure 9 shows the distribution of mean surface temperature for the selected time period 13:04. A distinguishable temperature distribution for roof, street, wall A and B can be seen. There are roughly concentric regions of high temperature on wall A, the center starting from the lower left corner. Similarly, the region of the street closest to wall A is also warm. These patterns might be related to the distribution of heat transfer coefficient caused by a canopy vortex. Several wind tunnel experiments[12)13)] , presented that the scalar transfer coefficient of windward wall of a 2D canopy increases with height. It indicates that the fresh air is introduced into the cavity along the windward wall and scalar boundary layer develops with downward motion of the canopy vortex. The tendency observed in wall A and street is consistent with their work.

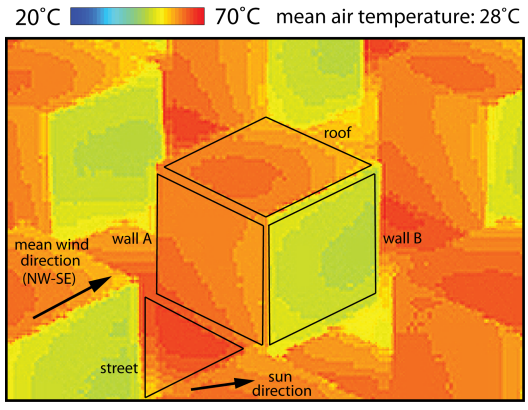

Fig. 9 Mean surface temperature distribution based on individual pixels. One-minute average, 13:04.

Surface temperature fluctuation denoted by the standard deviation of each pixel is depicted in fig. 10. Different patterns can be seen for each surface. The roof area shows the highest value and a directional gradation from the lower right corner can be seen. In contrast, the value at the lower part of wall A, wall B, and street are much smaller than that of the roof. It may be due to the difference of wind speed close to each surface. According to Oke[14)] , the flow regime of this array with density of 25% can be classified as skimming flow. It indicates that the flow within canopy is relatively week, and part of it cannot enter the cavity.

Detailed pattern of distribution of standard deviation for each period shows different tendency. Although the data of other periods are not included here, the correspondence of the pattern and background conditions of velocity and radiation was examined. However, we could not find a clear association between this pattern and the ambient conditions, and that remains a point to be elucidated in future investigations.

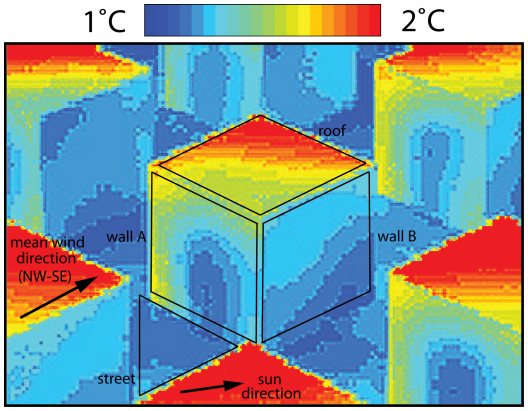

Fig. 10 Spatially averaged standard deviation based on time series data of each pixel for covered obstacles. One-minute average (13:04). Mean wind speed of 0.39 m/s, global solar radiation of 757 W/m^2, and air temperature of 27.7℃.

Figures 11 and 12 show the spatially-averaged standard deviation of surface temperature for roof against wind speed and its standard deviation, respectively. The data of three averaging periods, 1min, 10s and 2s, were compared. With 1 min averaging, surface fluctuation is sensitive to weak wind conditions.

The standard deviation of 2s is very small regardless of the wind condition and almost same as the resolution of the infrared camera. It implies that the measurement setting of our study cannot detect the instantaneous fluctuation of surface temperature due to turbulence with a time scale of 2s. In contrast, the standard deviation of 10s shows larger values than that of 2s, and it increases with the increase of standard deviation of wind speed,

although the plots are scattering. It is due to the influence of turbulent airflow above the array. The values of 1min are much larger than the others and almost insensitive to both mean wind speed and standard deviation. The reason of this tendency might be atributted to the effect of fluctuation of solar radiation. Although the data selected for analysis was based on the criteria of standard deviation of solar radiation lower than 3 W/m^2, the response time of the pyranometer is 17s, thus it is probable that the actual solar radiation fluctuated stronger compared with the recorded data. Eventually, the time scale of 10s seems to be most suitable for the analysis of surface temperature fluctuation affected by turbulent airflow. Since the size of the cube and the whole array are 0.10m and 1m respectively, wind speed close to the array lower than 0.01 m/s or 0.1 m/s may be desirable to capture the event of flow passing through a block or the whole area of the array. Unfortunately, such a condition is very rare in the daytime. For this reason, in future investigations using larger obstacles might be more appropriate for capturing flow events. Nevertheless, the fact that the infrared camera can capture very small temperature fluctuations and give a visual output is an interesting point that opens possibilities of further study

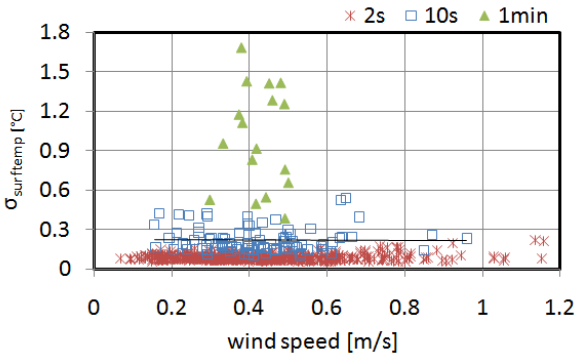

Fig. 11 Spatially averaged standard deviation of roof surface temperature plotted against wind speed. One minute average, exp01 and exp02.

3.4 Temperature profile above the roof

The normalized temperature profile above the roof is shown in figure 13. It is based on one-minute averaged data measured by fine-wire thermocouples at 1mm, 5mm, and 10mm for the entire period of exp01 and exp02. The most evident fact is the decreasing temperature with height. However, temperature at 5mm shows the longest horizontal spread, followed by 1mm and 10mm.

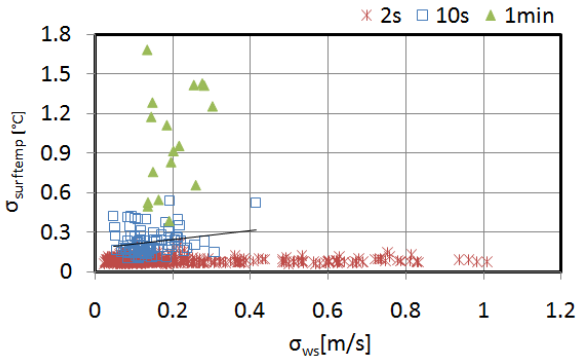

Fig. 12 Spatially averaged standard deviation of roof surface temperature plotted against the standard deviation of wind speed. One minute average, exp01 and exp02.

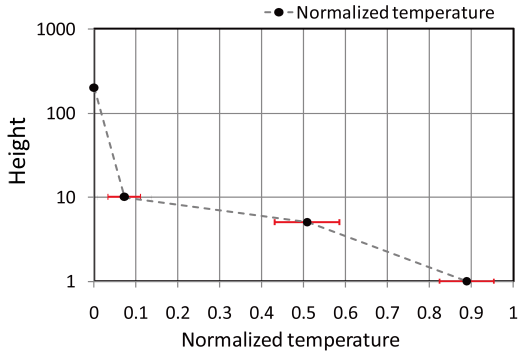

Fig. 13 Normalized temperature (x-axis) profile above the roof of an obstacle for the entire period of exp01 and exp02. Red lines represent standard deviation.

Figure 14 shows the instantaneous temperature fluctuation at each measured height, defined as the difference between instantaneous value and time averaged value. The temperature at height of 1mm and 10mm fluctuate approximately by ±5℃ and ±8℃, respectively. In contrast, the temperature variation at a height of 5mm is the largest among the three. Under particularly calm wind condition, the strongest fluctuation of temperature at 5mm is more remarkable. At that height, we could find a sharp increase followed by a rapid decrease during the period from 31s to 34s. Since the wind speed is less than 0.2m/s and the temperature difference between the roof surface and air at 2H is about 35℃, such conditions implies that natural convection is dominant (the Grashof number is approximately $5.6 \cdot 10^{10}$). Therefore, the sharp fluctuation measured at 5mm might be related to a hot plume arising from the warmed roof surface. The rea-

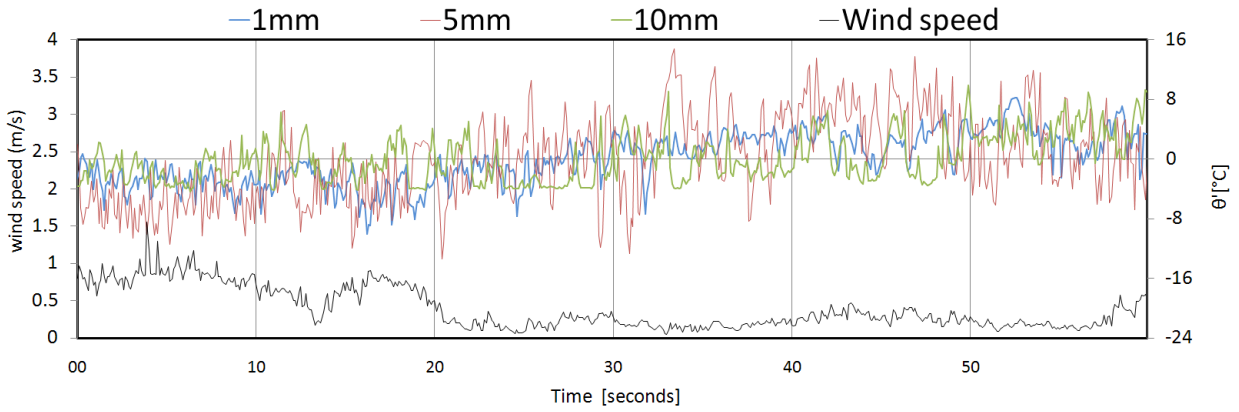

Fig. 14 Temperature fluctuation measured at different heights by fine-wire thermocouples plotted against wind speed for a selected interval of one minute (13:04).

son why the fluctuations of other two heights are weaker than that at 5mm is probably caused by the following fact. In the near roof region, hot plumes are intermittently generated with a subsequent descending of cool air. Hence, temperature at 1mm, too close to the surface, might be dominantly affected by surface heating, and less sensitive to the cold downward motion. Air at 5mm is probably easy to move because of the larger distance from the roof and more flexible air motion. In contrast, at 10mm it is too far to be affected by the ascending hot plume motion.

4. Conclusions

A method to analyze surface temperature distribution and its fluctuation due to air flow was investigated using infrared thermography. Outdoors measurements of surface temperature of a cubical array showed the similarity between surface temperature and scalar transfer coefficient, although we could not make definite conclusions about why some patterns of standard deviation arose. This is a point to be elucidated in future investigations. We also found that 10s averaging period may be appropriate for the analysis of surface temperature fluctuation affected by turbulent airflow, and we suggest that a larger model is desirable if the same materials are used.

Using high responsive thermocouples in the near-wall region of a block surface, we found that under particularly calm wind condition, air temperature fluctuation at 5mm has the strongest fluctuation, which may be related to a hot plume arising from the warmed surface.

This work, as a first approach, shows a promising method for analyzing surface temperature characteristics of urban-like block arrays.

Acknowledgments

This research was financially supported by a Grant-in Aid for Scientific Research from the Ministry of Education, Science and Culture of Japan.

References

1) Grimmond C.S.B., Progress in measuring and observing the urban atmosphere, Theoretical and Applied Climatology, 84, p.3-22 (2006).

2) Kanda M., Progress in the scale modeling of urban climate: Review, Theor. Appl. Climatol., 84, p.23-33 (2006).

3) Aida M., Urban albedo as a function of the urban structure - A model experiments, Boundary-Layer Meteorology, 23, p.405-413 (1982).

4) Oke T.R., Canyon geometry and the nocturnal urban heat island: comparison of scale model and field observations, Journal of Climatology, 1, p.237-254 (1981).

5) Kanda M., Kawai T., Kanega M., Moriwaki R., Narita K., Hagishima A., Simple energy balance model for regular building arrays, Boundary-Layer Meteorology, 116, p.423-443 (2005).

6) Pearlmutter D., Berliner P., Shaviv E., Evaluation of urban surface energy fluxes using an open-air scale model, Journal of Applied Meteorology, 44, p.532-545 (2005).

7) Yee E., Biltoft C.A., Concentration measurements in a plume dispersing through a regular array of obstacles, Boundary-Layer Meteorology, 111, p.363-415 (2004).

8) Macdonald R.W., Griffiths R.F., Cheah S.C., Field experiments of dispersion through regular arrays of cubic structures, Atmos. Environ, 31, p.783-795 (1997).

9) Cheng H., Castro I.P., Near wall flow over urban-like roughness, Boundary-Layer Meteorology, 104(2), p. 229-259 (2002)

10) Kovar-Panskus A., Moulinneuf L., Savory E., Abdelqari A., Sini J.F., Rosant J.-M., Robins A., Toy N., A Wind Tunnel Investigation of the Influence of Solar-Induced Wall-Heating on the Flow Regime within a Simulated Urban Street Canyon, Water, Air, & Soil Pollution: Focus, 5-6(2), p.555-571 (2002).

11) Astarita T., Cardone G., Carlomagno G.M., Infrared thermography: An optical method in heat transfer and fluid flow visualization, Optics and Lasers in Engineering, 3-4, p.261-281 (2005).

12) Narita K., Experimental study of the transfer velocity for urban surfaces with a water evaporation method, Boundary-Layer Meteorology, 122(2), p.293-320 (2006).

13) Aliaga D., Lamb J., Klein D., Convection heat transfer distributions over plates with square ribs from infrared thermography measurements, International Journal of Heat and Mass Transfer, 37(3), p.363-374 (1994)

14) Oke T., Street design and urban canopy layer climate, Energy and Buildings, 11(1-3), p.103-113 (1988).